[To Index]

EFFECT OF REAL PARTICLES PACKING WITH LARGE SIZE RATIO ON POROSITY AND TORTUOSITY OF FILTER BED

Mota, M.*, Teixeira, J.A., Dias, R. and Yelshin, A.
Centro de Eng. Biológica – IBQF, University of Minho, Campus de Gualtar, 4710-057 Braga, Portugal
*Email Address: MMota@reitoria.uminho.pt
Telephone: +351 253 601191 Fax: +351 253 678986

Abstract: The complexity of processes involved in the formation of granular beds results in limited information about permeability k, which directly rela tes with packing porosity e and tortuosity T. For a mixed bed of particles significantly different in size, the influence of packing affects permeability. For a better understanding of the underlying relationship between k, e, and T in mixed beds of particles significantly different in size, simplified porous media model of binary mixture of spheres were used. Boundary analysis of the binary packing showed that the approach based on the fractional porosity of large and small size particle fractions gives a tool for e control. This approach allows a new insight into the mixture structure and provides explanation for the different types of the obtained porosity. Binary packing of glass beads with size ratios 13.3, 20, and 26.7 were investigated. As a basic relation for the dependence of T on e, at different volume fraction x_D of large particles in the mixture, the formula $T = 1/e^n$ was used. The obtained experimental results show that the parameter n is a function of the packing content x_D and may vary in the range of 0.4 – 0.5. The reason for n variation was explained by the wall effect of the small particles arrangement occurring near the large particles surface. A model accounting for this effect is proposed and may be useful for transport phenomena analysis in granular bed filters.

Keywords: binary mixture, porosity, particle size ratio, tortuosity, permeability

1. Introduction

Models of behavior binary particle beds porosity vs. the volume fraction on of the mixture components were described in many publications [1-9]. Nevertheless, models of fluid flow or mass transfer in porous media need to establish relationships of packed bed porosity with tortuosity, permeability or diffusivity [10]. For a mixed bed of particles significantly different in size taking into account the influence of the porosity on the permeability through such characteristic as tortuosity becomes important [11].

Particularly, in solid-liquid separation the knowledge of solids packing structure is important to control permeability and dewaterability. For instance, cakes are formed in filtration often represented by the composition in coarse and fine particles. Similar composition is also observed in filter and catalyst beds.

To clarify the relationship between packing porosity, tortuosity, and permeability, binary mixtures of spheres of different size are investigated and analysed in the current work.

2. Background

The permeability k of filter bed is usually characterised by measuring the flow velocity at fixed pressure drop in laminar regime, $u = k \cdot \Delta p / (mL)$, where k is the permeability, Δp is the pressure drop, L is the bed thickness; m is the liquid viscosity. The permeability itself is a complex function of some variables: e, d_{av}, T

$$k = d_{av}^2 e^3 / \{36 K_0 T^2 (1-e)^2\} \tag{1}$$

where d_{av} is the average particle size in the bed and for binary mixture of large particles of size D and small of d is $d_{av} = \{x_D / D + (1 - x_D) / d\}^{-1}$; x_D is the volume fraction of large particles in the bed; complex $K_0 T^2 = K$ is the Kozeny's coefficient and for granular beds

$K = 4.2 \div 5.0$; T is the tortuosity; K_0 is the shape factor depending on a capillary pore cross-section area shape: for spheres packing $K_0 = 2.0$.

The tortuosity is defined as $T = L_e / L$, where L_e is the average flow pathway length and L – the bed thickness. In general, the tortuosity depends on the mixture content and, respectively, on the overall porosity e: $e = e(x_D)$ and $T = T(e)$ [10].

2.1. Porosity

Below we will use a model of the binary mixture developed [10] in previous research [10,12-14]. This model makes possible to analyse the influence of each particle fraction on the overall porosity in all range of x_D by means of a fractional porosity approach.

Let us represent the overall porosity e as a function of fractional porosity $e_D = e_D(x_D)$ and $e_d = e_d(x_D)$, where e_D is the void fraction of large particles in the total volume of the mixture, and e_d is the specific void fraction of small particles in the remaining void volume of the mixture. Since the overall volume of solids in the mixture, $1-e$, is a sum of volumes of large particles, $1-e_D$, and small particles, $(1-e_d)\cdot e_D$, the porosity of the mixture becomes, [14],

$$e = e_D \cdot e_d \tag{2}$$

Example of e_d and e_D together with e for moderate particle size ratio are shown in Figure 1a, curves 1, 2, and 3, respectively. Dependences were built based on model obtained [10] for $D/d \sim 10$.

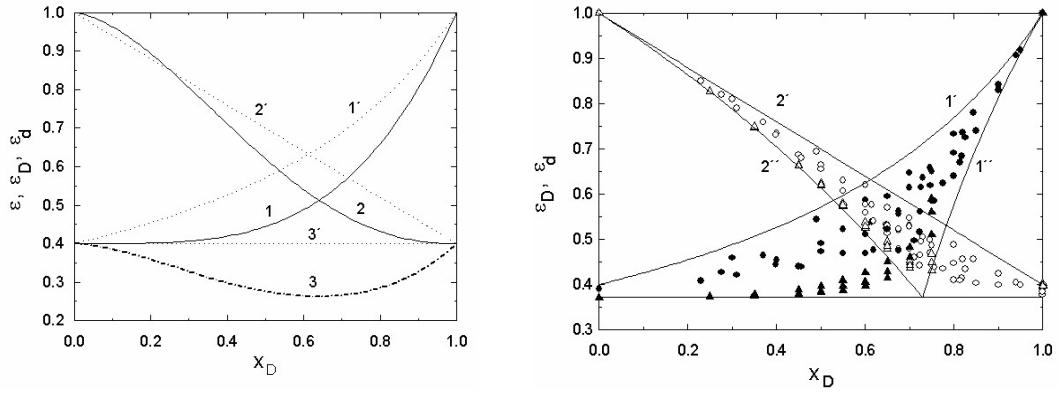

(a) (b)

Figure 1. Representation of the binary mixture porosity $e(x_D)$ by fractional porosities $e_D(x_D)$ and $e_d(x_d)$. (a) – Sketch of e (3 and 3′) and fractional porosities 1,2 and 1′, 2′ drawing for moderate particle size ratio $d = d/D \sim 0.1$ (curves 1 – 3) and $d/D = 1.0$ (curves 1′- 3′). (b) – Sketch of fractional porosities drawing for particle size ratio $d/D \to 0$ (curves 1′′ and 2′′ and horizontal line). Points correspond to experimental data for a d/D range 0.0375 – 0.513 obtained in [10] and in the present work. Open and solid symbols correspond to e_D and e_d, respectively.

At limit d/D = 1.0, fractional porosities e_d and e_D represent curves 1′and 2′ and e corresponds to line 3′ in Figure 1a. At the other extreme $d/D \to 0$, in idealized case, e_D and e_d are characterised by two parts: curve 1′′ and 2′′, respectively, and segment of horizontal line, Figure 1b, if we assume that $e_d^0 = e_D^0$. Here e_d^0 and e_D^0 are the porosity of the bed of pure small and large size particles, respectively.

For the limit $d/D \to 0$ when $e_D = e_D^0$ and $e_d = e_d^0$ the model (2) takes the form of equations (3) – (5) [10], which is a case of a conventional boundary limit of the binary mixture with significantly different particles size [1,2,7,15].

$$\begin{cases} e_d = (e_D^0 + x_D - 1)/(e_D^0 x_D), & x_D \in [x_{D\min}, 1] \\ e_d = e_d^0, & x_D \in [0, x_{D\min}] \end{cases} \tag{3}$$

$$\begin{cases} e_D = (1-x_D)/(1-e_d^0 x_D), & x_D \in [0, x_{D\min}] \\ e_D = e_D^0, & x_D \in [x_{D\min}, 1] \end{cases} \quad (4)$$

with minimum porosity $e_{Min} = e_d^0 \cdot e_D^0$ at

$$x_{D\min} = (1-e_D^0)/(1-e_d^0 e_D^0) \quad (5)$$

The influence of small and large particles arrangement on the shape of the overall porosity dependence was discussed in the work [16], where it was shown that continuity or discontinuity of e_D and e_d dependences are the result of packing effects in the region of $x_{D\min}$. These effects are caused by small particles wedging between large particles in the skeleton and by disturbance nearby the surface of large particles.

2.2. Tortuosity

Tortuosity is associated with the flow and mass transfer characteristics such as permeability, diffusivity, effectiveness, etc. [17-27].

The tortuosity investigations have concentrated on the establishment of a relationship between the overall porosity and tortuosity, T, [28]. For granular packing the main effort has been devoted to determine some fixed tortuosity value, [9,29-31]. Limited information is available on the overall tortuosity performance in the region of minimum porosity.

Theoretical and practical investigations show that the tortuosity of a granular bed depends on fractional content, porosity, and on particle shape. Tortuosity increases with decrease of the ratio $d = d/D$. Therefore the value of T may vary in a wide range [10,12-14,32].

Among a variety of proposed dependences T vs. e a simple relation is often used

$$T = 1/\{e(x_D)\}^n \quad (6)$$

where n is a constant usually between 0.4 and 0.5.

There is evidence in living tissue that the dependence of the tortuosity does not follow equation (6) with constant value of n. Moreover, it was observed a dependence of n on e [33]. The above-mentioned observation requires experimental verification, due to its importance as a correction factor, in the Kozeny – Carman model, of the packing bed permeability and usefulness for further transport phenomena analysis in granular beds. Moreover, experiments and theoretical analysis show that the tortuosity variation in granular beds is limited by fractional porosities values. Theoretically, if the dependence (6) is used, the maximum binary mixture tortuosity corresponds to $T = 1/e^n = 1/(e_D e_d)^n$ [14,34]. Because the tortuosity increases when the porosity decreases, our attention would be focused on packing with small particle size ratio, i.e. $d \leq 0.1$.

2.3. Permeability

The porosity has a significant effect on the permeability. As an example the permeability of the binary glass beads packing (D/d = 10.22) is show in Figure 2a.

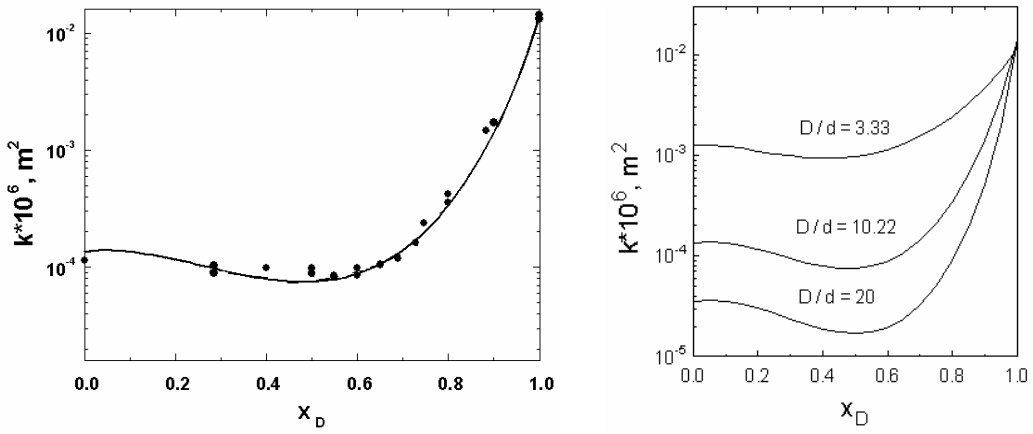

(a) (b)

Figure 2. Permeability k dependence on x_D. (a) – Experimental (points) and modelled (curve) permeability k from [10], D/d = 10.22, $e_D^0 = e_d^0 = 0.4$, and $T = 1/\{e(x_D)\}^{0.4}$. (b) – Simulated k by the model [10] for different D/d. Large particles size is fixed and assumed to be D = 3.45·10^{-3} m.

Simulation of k vs. x_D for a fixed D confirms that the ratio d affects the permeability whenever we change the size d, Figure 2b. The depth of the minimum region of the k profile increases as d decreases and is re-located in the range of $x_D \sim 0.2$ - 0.7 to $x_D \sim 0.3$ - 0.6.

It is possible to show that in different packing conditions the monosized packing porosities e_D^0 and e_d^0 significantly affect the permeability profile, Figure 3. Simulation was done using the model presented in [10] for a packing of $D/d = 10.22$ ($D = 3.45 \cdot 10^{-3}$ m). The dashed curve in Figure 3 represents the conventional case of $e_D^0 = e_d^0 = 0.4$.

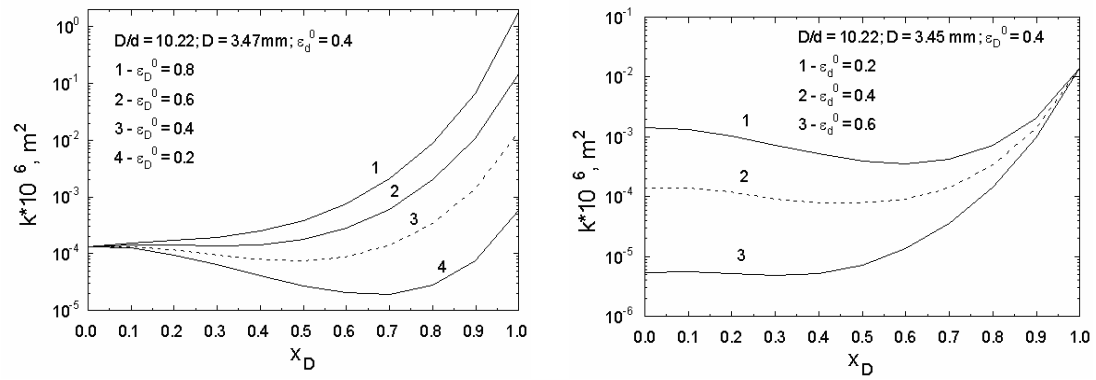

Figure 3. Dependence of the permeability k on x_D and monosized packing porosities for $D/d = 10.22$: (a) e_D^0 = var. (b) e_d^0 = var. The dashed curve belongs to a conventional case of $e_D^0 = e_d^0 = 0.4$.

As we can see, the permeability is very sensitive to the porosity and particles size; even with exactly the same fractional porosity, the permeability may be changed by more than one order of magnitude.

3. Materials and Experimental Procedure s

The particle composition [35] and the packing method affect the properties of mixed beds [10]. D ifferent packing methods imposed different packing constraints, which in turn affected the degree of randomness of packing [36]. Therefore many researchers devoted a lot of effort to develop packing methods that could give rise to reproducible packing beds [9,31,37-39]. This fact was the reason for developing a column packing procedure of binary glass beads mixture that give consistent results.

Binary mixtures of glass beads were used in all experiments included in the present work: Beads of large size were obtained from *Simax*. The other glass beads came from *Sigmund Lindner*. Particles density was 2500 kg/m^3 in every case.

3.1. Testing mixing and packing procedure

In order to eliminate segregation effect of particles significantly different in size during mixing and packing a viscous water solution of glycerol was used Application of glycerol for particles adhesion on the later stage of mixture packing gives the possibility of removing adhesive from a column with a minimum cost, simply by washing with water. Preliminary experiments show that the optimal solution for mixing is the 90% solution of glycerol in water.

The procedure includes mixing the glass beads in the appropriate proportion with a glycerol aqueous solution, filling the column, packing the column, washing the glycerol out, followed by a check-up by means of image analysis particle fractions distribution in the column.

To check homogeneity and reproducibility of the method a square column (5 cm inner side and 40 cm high) was used in the experiments. To provide better image analysis of particles distribution glass spheres of different size were marked with waterproof inks of different colours.

A certain mass proportion of dyed spheres were put in a mixer, Figure 4a. A solution of 90% glycerol in water was then added to the spheres in a 15% mass proportion. Spheres and

glycerol solution were mixed at 75 rpm during 5 minutes inside the vessel. Finally, the sticky mixture with sufficient adhesion between spheres was obtained.

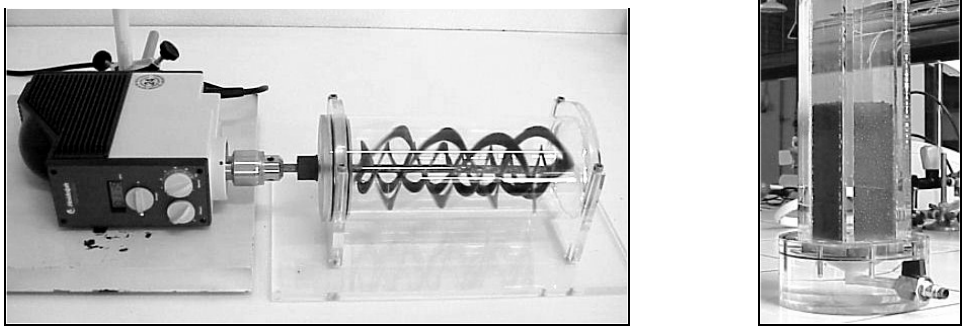

(a) (b)

Figure 4. Equipment used for tasting mixing procedure. (a) Mixer. (b) View of the square column with a binary packing.

The mixture was the transferred to a prismatic vessel and glycerol was washed out, Figure 4b. Mixtures with particle size ratio D/d = 13.3, 20, and 26.7 were tested covering the range of x_D from zero to 1.0. Digital pictures taken from each face were automatically treated by image analysis to determine the coloured fraction present in each face, Figure 5a.

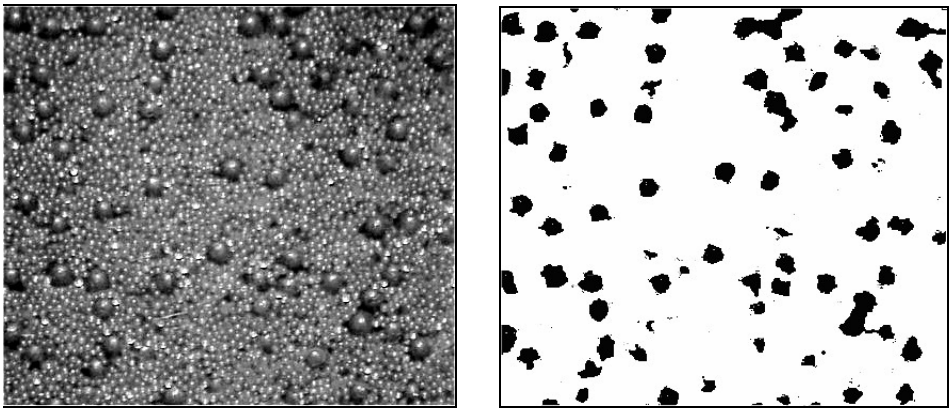

(a) (b)

Figure 5. Example of image treatment of a binary packing. The mixture contains 30% of 3mm spheres (black) and 70 % of 0.875 mm spheres (grey). (a) Picture taken from one of the column sides. (b) Treated image of the picture (a).

The homogeneity of particles distribution was checked by comparing the large size particle fraction area displayed in the images with the fraction x_D of the particles presented in the mixture poured to the column. Statistical analysis showed that no significant deviation existed in the colour distribution of each of the four faces. A chi-square test showed that a uniform distribution could be accepted for the beads at the 1% significance level, no segregation of bead size nearby the edges was observed and that no column wall effect was present. The two-dimensional picture obtained by image analysis was converted to the corresponding 3-dimensional distribution, from which the expected bed porosity was inferred.

The estimated porosity was compared with the experimental value determined by gravimetry. Hundreds of experiments performed with this method showed the high reproducibility of the method. The standard deviation obtained for each face varied between 0.12% and 1.42%. The mean standard deviation obtained was 0.89%. Therefore, we may say that the results obtained are reproducible and that no significant variation occurs in the captured image distributions of the four faces. More information about the method is given in a previous work [40].

3.2. Porosity and permeability measurements

For the binary packing of particles of different size, the experimental method for measurement of porosity e and permeability k as well as a data treatment procedures are described in [10,13,32,40].

Binary beds with particle of size ratio D/d = 13.3, 20, and 26.7 were object of the investigation.

The permeability was calculated by measuring flow velocity at a fixed pressure drop in laminar regime. Using experimental porosity and average particle diameter in the mixture d_{av}, the tortuosity may be calculated from the formula (1).

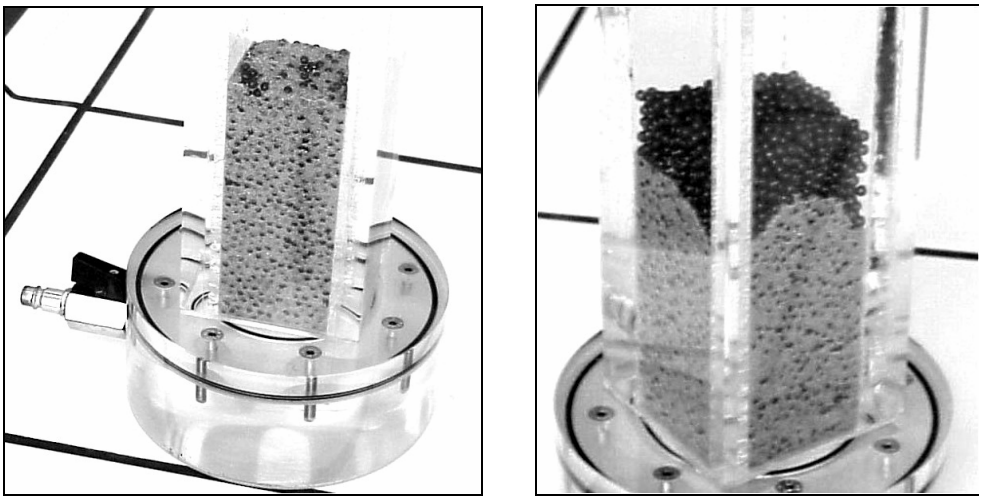

(a) (b)

Figure 6. Packing in the region of minimum porosity (a) and packing enriched of large size particles (b). (a) - Mixture with 70% of 4 mm (black), 30% of 0.375 mm (gray) spheres. (b) – Mixture contains 75 % of 4 mm spheres (black) and 25% of 0.375 mm spheres (grey). The packing staying below the segregation zone corresponds to the complete packing at the minimum porosity region.

This investigation was mainly concentrated on packings with x_D up to the region of minimum porosity, because after that a complete packing, Figure 6a, transforms spontaneously in a segregated packing, Figure 6b.

4. Results and Discussion

4.1. Porosity

For binary mixtures with particle of size ratio D/d = 13.3, 20, and 26.7, in the context of the fractional porosity, all values of e_d and e_D are encompassed by the corresponding regions defined by the model displayed in Figure 1b. With decreasing d, fractional porosities (represented by triangles) behave similarly to the linear model, equations (2) – (5), but in the range of minimum porosity they are still quite far from the model prediction.

Experimental data in Figure 7a show two types of porosity behaviors: at $d \geq 0.1$ a smooth transition in the region of minimum porosity is observed, whereas for lower d the porosity performs more likely as predicted by equations (2) – (5), Figure 7a, curve 3. The above-mentioned segregation effects (may be the reason why the smooth transition observed in the region of minimum porosity changes to a sharper transition when d becomes smaller than 0.1. It seen, also, that the previous model has limitations in the range of $D/d > 10$ [10], curves 1 and 2.

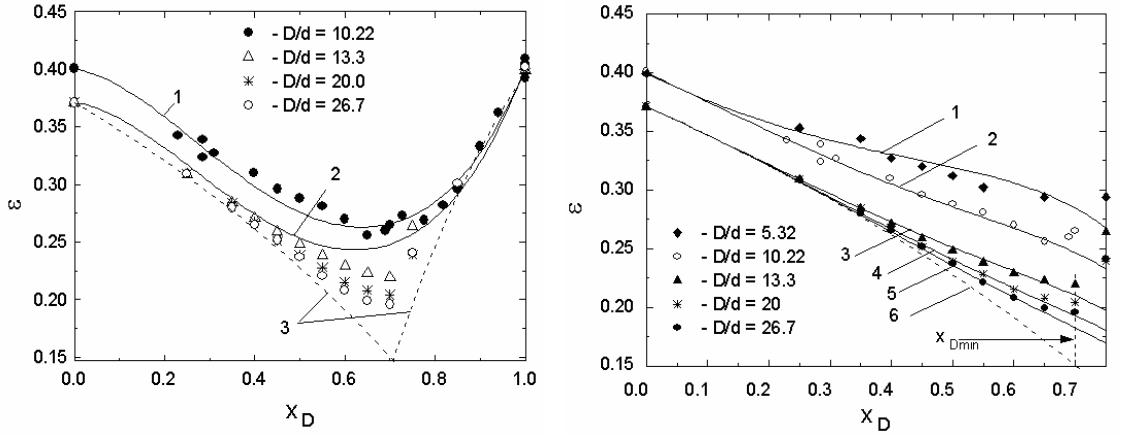

(a) (b)

Figure 7. Measured (points) and simulated (curves) porosity at different particle size ratio. (a). Curves 1 (D/d = 10.22) and 2 (D/d = 13.3) – Model [10]; 3 – Equations (2) – (5) at $d \to 0$, for measured $e_d^0 = 0.371$ and $e_D^0 = 0.4$. (b). Comparison of the experimental porosity with the model (8). 1 – 5 Model (8) for D/d = 5.32, 10.22, 13.3, 20, and 26.7, respectively. 6 – Equation (7).

Nevertheless, for d < 0.1 we tried to us the approach similar to [10], i.e. to apply a correction function. As mentioned above, practical interest represents complete packings in the region $x_D \le x_{D\min}$. In this case, the system (2) – (5) transforms to the equation

$$e = e_d^0(1-x_D)/(1-x_D e_d^0), \qquad x_D \in [0, x_{D\min}] \tag{7}$$

A correction function $j(d)$ was searched in the form of $e = e \cdot j(d)$, where e is defined by equation (7). The best result was obtained for a correction function of the form $j(d) = \exp(1.2264 x_D^{1/\sqrt{d}}) = \exp(1.2264 x_D^{\sqrt{D/d}})$, hence, equation (7) has the following form

$$e = e_d^0(1-x_D)\exp(1.2264\, x_D^{1/\sqrt{d}})/(1-e_d^0 x_D) \tag{8}$$

that is valid for $x_D \le x_{D\min}$.

Function (8) gives good results, Figure 7b, up to the composition with minimum porosity. When the d value approaches zero $j(d) \to$ 1.0, the model gives rise to the "ideal" curve given by equation (7). The validity of this correction function can be accepted for $d \le 0.1$.

Minimum Porosity. The minimum porosity, $e_{\min}$, depends on the particles size ratio D/d. The porosity $e_{\min}$ decreases when the size ratio increases and converges to the absolute minimal value, e_{Min}, for $D/d \to \infty$ [14,41]. When $D/d \to \infty$ ($d \to$ 0) the

displacement or distortion effects of each particle fraction on fractional porosities become insignificant. Hence, the absolute minimal porosity is defined by the relation $e_{Min} = e_D^0 \cdot e_d^0$.

In reality, the minimum porosity is $e_{\min} \geq e_{Min}$. By substituting (8) in (7) we have

$$e_{\min} = e_d^0 (1 - x_{D\min}) \exp(1.2264 x_{D\min}^{1/\sqrt{d}}) / (1 - e_d^0 x_{D\min}) \tag{9}$$

Experimental values of the minimum porosity obtained in our work (solid circles 1) are shown in Figure 8 together with equation (9) calculated for measured e_d^0 = 0.371 and e_D^0 = 0.4, curve 1. As can be seen, the function (9) underestimates the minimum porosity of the experimental data. This fact leads to the conclusion that even at d = 0.037 the measured fractional porosity (Figure 1b) is quite far from the case of $d \to 0$, equations (3) and (4).

In the context of the dense and loose packings it is useful to analyze the dependence of $e_{\min}$ on d taken from several literature sources. Figure 9 represents a data collection containing current research data (points 1) as well as data gathered from different researchers.

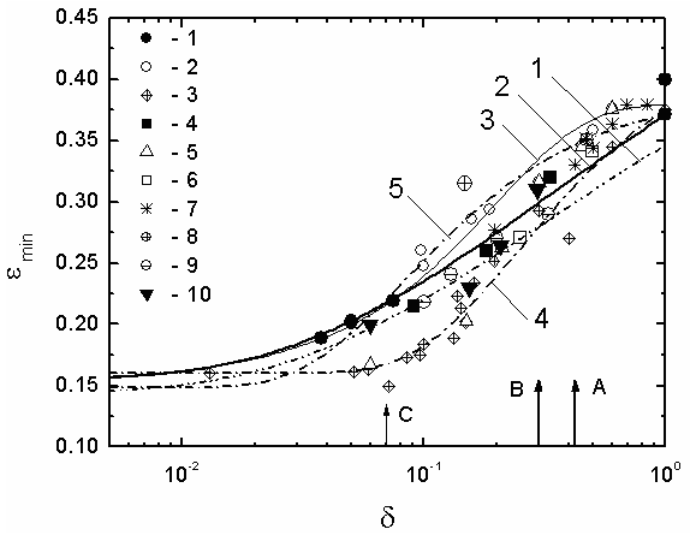

Figure 8. Dependence the spheres binary packing minimum porosity $e_{\min}$ on the particle size ratio d. Experimental data: 1 – Current work; 2 – Data [10]; 3 – Data [41]; 4 – Data [42]; 5 –

Data [2]; 6 – Data [7]; 7 – Data [9]; 8 – Data [43]; 9 – Data [44]; 10 – Data [45]. Curves: 1 – Equation (9); 2 – Corrected function (9) with a = 1.045, 3 – Boltzmann fit; 4 and 5 – Relation from [41] for e_{Min} = 0.16, e_d^0 = 0.375 and e_{Min} = 0.1484, e_d^0 = 0.375, and exponential coefficient 0.085, respectively.

We can see that experimental data scatter between dense packing represented by the data points 3 (McGeary quoted from [41]), loose packing (points 2) and current experimental data (points 1).

In Figure 9, relation from [41] for e_{Min} = 0.16 and e_d^0 = 0.375 is shown as curve 4. An attempt to adopt this relation for a loose packing (curve 5), leads to replace an exponential coefficient 0.25 with 0.085 but in comparison with Boltzmann fit it gives a worse fitting with experimental data at $d \sim 1$ and $d << 1.0$. Therefore, our choice was favorable to the Boltzmann fit.

Experimental data in Figure 8 clearly differentiate zones for d related with specific packing mechanisms. One of the possible effects on the packing is the so-called wall effect. The large size particles are "viewed" by the small ones as a "wall". If we assume that the main effect on $e_{\min}$ is related with the fractional porosity of small particles, which in this case is larger than e_d^0 then we can improve equation (9) by introducing a correction coefficient $a \geq 1$ in the form $e_{dc}^0 = a \cdot e_d^0$. For a = 1.045 (e_d^0 = 0.371), Figure 8, curve 2, equation (9) fits well to experimental data obtained in the current work.

Usually the disturbance or "wall" effect propagates to a distance of 4 – 5 diameters from the wall and may serve as an explanation for the observed dependence of e on $d = d/D$. Moreover, according to Figure 8, $e_{\min} < e_{Min}$ and if we want to have an almost completely undisturbed porous medium, the small particles will have to be about 140 times smaller than the big particles. In turn, for d > 0.07, the wall effect occurs in the whole pore void.

Finally, four regions on the dependence of $e_{\min}$ vs. d can be identified: 1). A region of d > 0.41 where a displacement mechanism acts upon particles (Figure 8, arrow A); 2). An intermediate region where a linear – mixing model is observed, for d = 0.2 (Figure 8, arrow

B); 3). A region of partially disturbed arrangement of small particles in the void of the skeleton, $0.007 < d < 0.2$ (Figure 9, arrow C); 4). A region of small particles arrangement close to the monosize packing, $d < 0.007$, $e_{\min} \approx e_{Min}$. In this case, the small particles can invade totally the internal void space of the large particles.

4.2 Tortuosity and porosity

The tortuosity in binary packing of particles with assumption of the relation (6) is

$$T = 1/(e_d e_D)^n = 1/e^n \tag{10}$$

and we must expect that according to the above discussed distortion effect the maximum tortuosity $T_{\max}$ is equal to

$$T_{\max} = 1/e_{\min}^n \tag{11a}$$

or, in the case of $d << 1.0$

$$T_{\max} \approx T_{Max} = 1/e_{Min}^n \tag{11b}$$

It must be admitted that the maximum tortuosity is usually observed in the region of minimum porosity. In Figure 9 are shown dependences of the porosity and tortuosity on x_D for three different types of binary mixtures: (a) – mixtures obtained in two-dimensional (2-D) simulation [12,46]; (b) – mixtures of glass beads; (c) – mixtures of glass beads with different types of kieselguhrs [13].

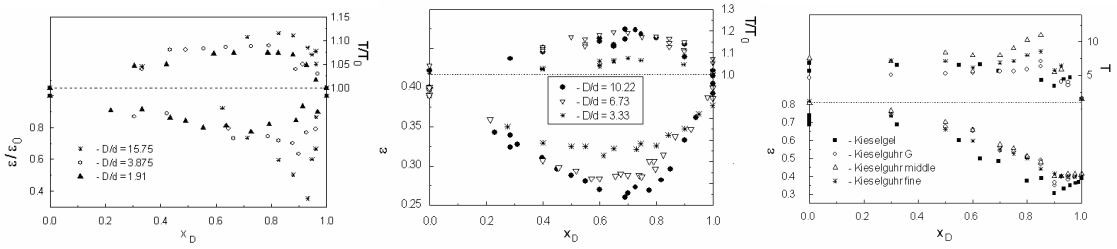

(a) (b) (c)

Figure 9. Dependences of e and tortuosity on x_D. (a). Normalised 2-D porosity e/e_0 and tortuosity T/T_0. (b). Mixtures of glass beads: e and T/T_0. (c). Mixtures of glass beads + kieselguhr (size ratio bead/particle 30 – 35): e and T. Values e_0 and T_0 correspond to the porosity and tortuosity of monosized packing.

The region of minimum porosity is characterised by a transition of pore size distribution from bimodal to unimodal [47]. Frequency distribution of different pore fractions obtained in 2-D binary mixture model are shown in Figure 10. The following pore fractions were considered: a). Pore of a throat size in the point of contact two small particles d, fraction 1, or large particles D, fraction 4, respectively; b). Pore of the throat size in the point of contact small, d, and large particle, D, fraction 2; c). Two other fractions include pores with size: (fraction 2) < Size < (fraction 4) = fraction 3, and Size > (fraction 4), fraction 5.

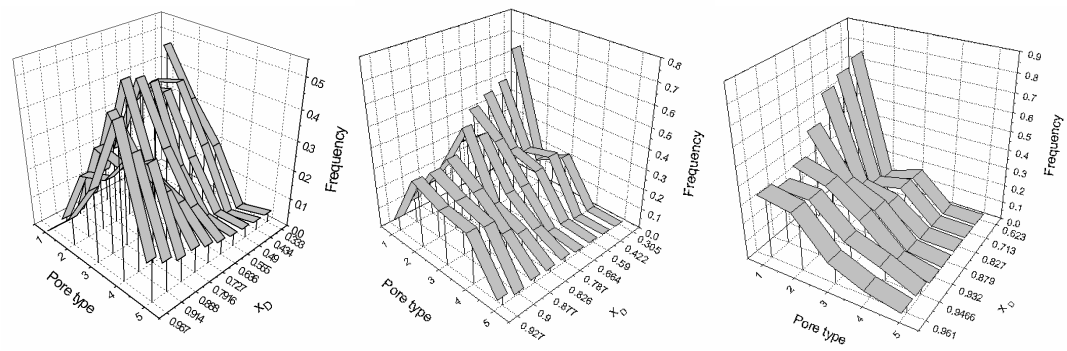

(a) (b) (c)

Figure 10. Histograms of a pore fraction distribution in 2-D binary mixture vs. x_D: (a) – Mixture with disksize ratio $D/d = 1.91$; (b) – Mixture with $D/d = 3.875$; (c) – Mixture with $D/d = 15.75$. Type of pore fractions (see the text).

The maximum tortuosity location in 2-D model correlates with the above-mentioned transition zone. With increasing of D/d the transition zone between bi- and uni-modal distributions moves toward larger values of x_D.

Before the discussion of new experimental data the following conclusions may be drawn. 1). The tortuosity of the binary mixed bed depends on the volume fraction of large particles x_D. 2). The tortuosity has limited change with increasing D/d, even for D/d = 10.22, T increases up to 20% of monosized bed packing of spherical particles, only, but tacking in account that $k \propto 1/T^2$ the miscalculation of the permeability with $T = const$ in the region of minimum porosity packing can be significant.

4.3. Permeability

In Figure 11a experimental data for k (size ratios D/d = 13.3, 20, and 26.7) are shown together with the permeability simulation (equations 1 and 6) using the porosity model (8) and assuming in (6) that n = 0.4 (dashed curves) or 0.5 (solid curves). The experimental data appears in between the simulation results. For x_D < 0.3, experimental and simulated values are closer for n = 0.5, whereas for x_D > 0.5 the model fits better the data with n = 0.4.

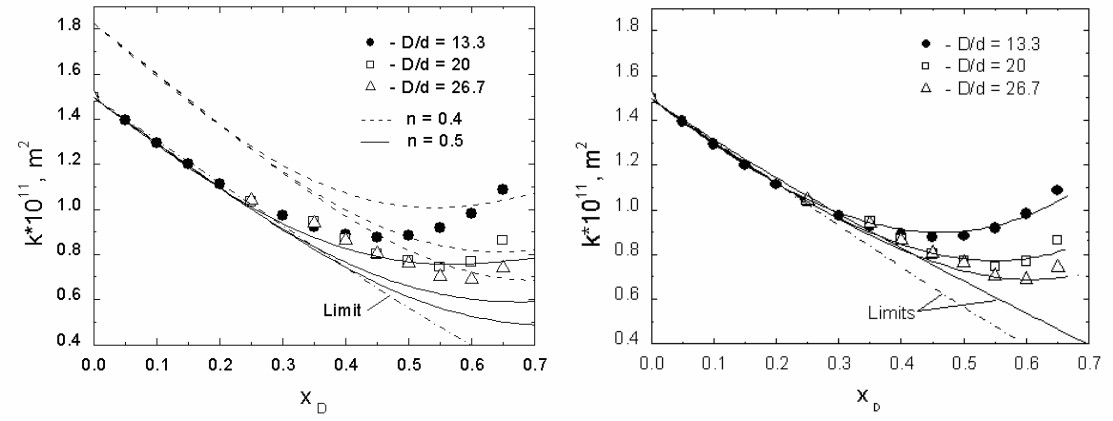

(a) (b)

Figure 11. Experimental and simulation results of $k(x_D)$ for binary packing of D/d = 13.3, 20, and 26.7. (a) – Model including equations (1), (6) and (8) with n = 0.4 and 0.5. The limit corresponds to $d \to 0$. (b) – Experimental and simulated permeability k vs. x_D when the parameter n in equation (6) is the function (14). Limits correspond to $d \to 0$ for n = 0.5 (dashed curve) and n given by function (14).

Discrepancy between predicted and measured tortuosity shows that the real average flow pathway is shorter than the theoretically expected. The reason for this is as the follows. For particles of significant difference in size, the wall effect near the large particles surface causes a bypass of part of the liquid through the less dense packing nearby the surface (distortion effect). Indirectly this is confirmed on 2D model, Figure 10, where changes in pore type distribution are observed.

The permeability deviation from the conventional model (6) with $n = const$ lead us to analyse the behaviour of parameter n in the range of complete binary mixtures, mixtures with $x_D \le x_{D\min}$ (mixtures with $x_D > x_{D\min}$ represent bi-layer systems and are out of the investigation). For the analysed cases of Figure 11a, the minimum porosity was achieved at $x_{D\min} \approx 0.7$ [16]. In assumption that the coefficient K_0 is almost constant and its variation is significantly smaller than the tortuosity (6), rearrangement of equation (1) gives

$$n = \frac{\ln\{36k\,K_0(1-e)^2/(e^3\,d_{av}^2)\}}{2\ln(e)} \tag{12}$$

For the ratios D/d = 13.3, 20, and 26.7, n values calculated based on the measured permeability are shown in Figure 12.

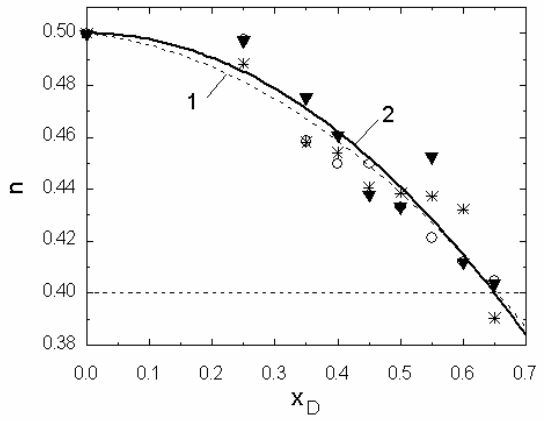

Figure 12. Dependence of n on x_D for data set of D/d = 13.3, 20, and 26.7 calculated by equation (12), points, and obtained correlation functions: 1 – parabolic fit, 2 – fitting function (14).

The parameter n of equation (3) in the range of provided experiments is between values 0.4 – 0.5. A fitting procedure between n and x_D gives a parabolic function $0.5 - 0.02637\,x_D - 0.19325\,x_D^2$, curve 1, with a regression coefficient of 0.97. As a simplified correlation the following parabolic formula may be proposed

$$n = 0.5 - ax_D^2 \tag{13}$$

that in our case fits well data at $a = 0.1/0.65^2 \approx 0.2367$, as seen on curve 2 in Figure 12

$$n = 0.5 - (0.1/0.65^2)x_D^2 \tag{14}$$

Simulation results with equation (1) are shown in Figure 11b, where the porosity is defined by (8) and the tortuosity is calculated using function (6) with the parameter n

modelled by (14). The model with the variable parameter $n = n(x_D)$ gives a good approximation of the experimental data. The comparison of the permeability profile in Figure 11b with Figure 11a leads us to the conclusion of the importance of the $n = n(x_D)$ approach for modelling binary packings with d < 0.1. Substitution of (14) into the limiting permeability relation ($d \to 0$) also shows a great effect on the permeability value.

Obtained results confirm the conclusion from [10,32] that the permeability has a minimum region which does not coincide with the porosity minimum value, and the region of minimum k becomes more concave with decreasing d .

4.5. Tortuosity and distortion effect near large particles surface

Decreasing n from 0.5 to 0.4 with increasing x_D to $x_{D\min}$ may be explained by the increase in the total surface area of large particles thereby increasing the fraction of the porous media involved in wall effect. When $d \to 0$ the volume involved in the wall effect will increase.

In spite of the scattering of the experimental data, as shown in Figure 13a, the proposed model gives a good trend for the tortuosity T vs. x_D.

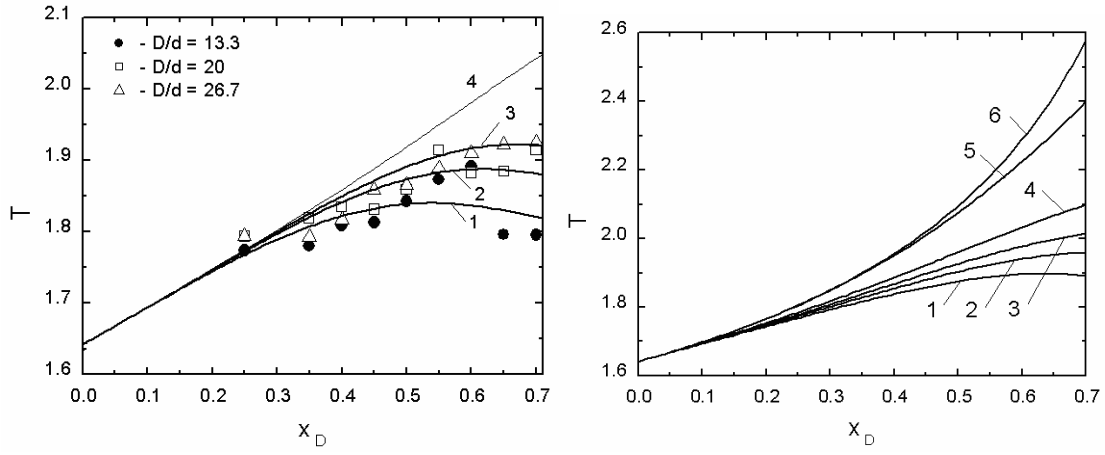

(a) (b)

Figure 13. Experimental (points) and simulated dependence of the tortuosity T on x_D ($x_D \le x_{D\min} = 0.7$). (a) – Curves 1 – 4 Modelling by equation (6) with the porosity function (8) and the parameter n by relation (14), where 4 is the case of the particle size ratio d = 0.01. (b) – Influence of the parameter n variation, equation (13), at different a on the tortuosity for d = 1/36 (curves 1 – 5): 1 – a = 0.278; 2 – 0.237; 3 – 0.204; 4 – 0.156; 5 – a = 0 (n = 0.5). Curve 6 corresponds $n = 0.5$ at $d \to 0$.

The effect of the a value on the tortuosity is shown in Figure 13b. When d = 1/36, a = 0 – 0.278 if we assume that the minimum porosity is reached at $x_{D\min}$ = 0.7, we can observe large changes in the tortuosity values as well as in the tortuosity profile if the packing quality is associated with the coefficient a in equation (13).

It is possible to have binary packing approaches to the "ideal" conditions when the wall effect is minimised:

(i). For certain d, the small particle packing within the skeleton void may approach to the regular, hence, $e \approx e_D^0 \cdot e_d^0$.

(ii). Non-spherical particles, for instance rod-like, have a less pronounced wall effect and therefore the liquid flow bypass through the zone close to the large particles surface may be reduced.

(iii). If the ratio d is small enough, the introduction into the binary mixture of a limited amount of a third particle fraction with particle size small enough to fill the void of the binary mixture may diminish the porosity irregularity. In this case, the mixture becomes ternary [12]. Something similar was observed in a cement paste-aggregate interfacial transition zone in a variety of concretes [48,49].

The above discussed effects of binary beds with particles of different sizes show that, to improve the quality of separation, attention must be paid to different aspects of packing. Parameters affecting permeability (e, d, T, etc.) show inter-dependence. Particularly in separation processes the tortuosity of filter media can affect the filter efficiency by two ways: 1) by inertial effect due to changing of flow direction in pore channels, and 2) by increasing with contaminants in porous media.

In order to illustrate main separation processes region application, we have used a fore-dimension graph, Figure 14. Typically, application regions of separation processes are overlapped. The same happens with using a theoretical background for these processes description. It can be illustrated with some examples: 1). Chromatography is applied to molecules and macromolecules separation as well as for virus, plasmids and bacteria separation. In some cases, a macromolecule may be considered as a micro-particle. 2). A modified adsorption model for microparticles is used in deep bed filtration models. 3). Membrane processes – in some models an assumption of a solvated ion as a spheric al particle is used and applied in modified filtration theory. 4). Ultrafiltration is applied for molecules and macromolecules separation as well as for microparticles (colloids) separation.

The complexity of separation processes description is due to numerous separating systems physico-chemical properties and porous media types variety. However, a term involving tortuosity should be applicable to the majority of porous media structure.

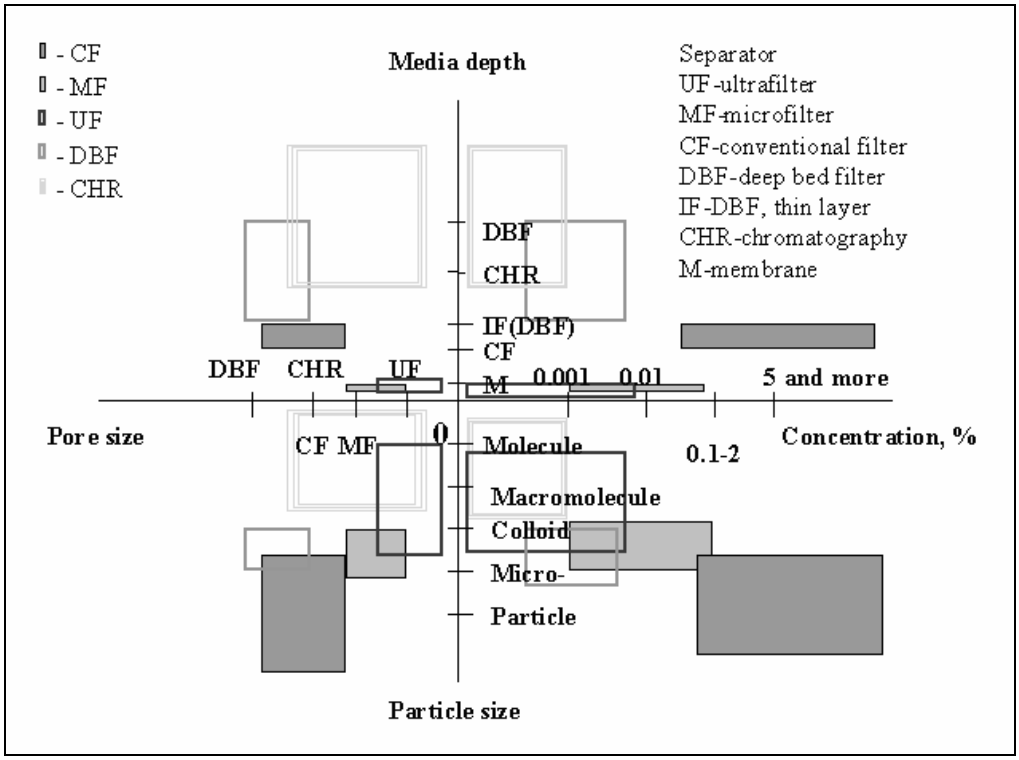

Figure 14. Scheme of separation processes with porous media application representing the following dimensions: pore size, porous media depth (thickness), handling concentration of separated substrates, and the size of separating substrates.

5. Conclusion

The complexity of processes involved in the formation of granular beds results in the inter-dependence of main parameters included in the permeability k, especially a packing porosity e and tortuosity T. The bed porosity in the region of minimum e is affected by particle size ratio d and packing fractional content.

According to results discussed above, 4 regions on the dependence of $e_{\min}$ vs. d can be identified: 1). A region of d > 0.41 where a displacement mechanism acts upon particles (Figure 8, arrow A). 2). An intermediate region where a linear – mixing model is observed, for d = 0.2 (Figure 8, arrow B). 3). A region of partially disturbed arrangement of small particles in the void of the skeleton, 0.007 < d < 0.2 (Figure 8, arrow C). 4). A region of small particles arrangement close to the monosize packing, d < 0.007, h > 0.90.

The developed approach is useful to understand binary mixture behaviors and shows that the approach based on the fractional porosity $e_D(x_D)$ and $e_d(x_D)$ may be a useful tool for the control of the overall porosity, giving a new insight on mixture structure and reasonable explanations for the different types of the porosity and tortuosity behavior in the region of the minimum porosity.

The obtained experimental results show that the parameter n in the formula $T = 1/e^n$ is a function of the packing content x_D and may vary in the range of 0.4 – 0.5. The reason for n variation may be explained by the wall effect of the small particles arrangement occurring near the large particle surface. A model accounting for this effect is proposed and may be useful for transport phenomena analysis in granular bed filters.

To understand how the wall effect diminishes with the increase in the particle size ratio in a binary mixture, additional theoretical and experimental investigations must be undertaken.

Acknowledgement

The authors acknowledge the grant that was given to Dr. Yelshin by Fundação para a Ciência e Tecnologia (FCT), without which this work would not be possible. The authors wish also to acknowledge the FCT funding of the project POCTI/EQU/37500/2001, under which the present research was performed. This project was partially funded by FEDER.

Nomenclature

a	correction coefficient for e_d^0 in the binary packing.
D	diameter of large particles (m).
d	diameter of small particles (m).
d_{av}	average particle diameter in the mixture (m).
D_{por}	pore diameter (m).
D_{th}	thought diameter (m).
K	Kozeny's coefficient.
k	permeability (m^2).
L	bed thickness (m).
L_e	average flow pathway length in the bed (m).
u	flow velocity (m/s).
n	power order in Equation (6).
T	tortuosity.
T_0	tortuosity of monosized packing.
x_D	volume fraction of large particles in the total volume of particles in the mixture.
$x_{D\min}$	volume fraction of large particles corresponds to the minimum mixture porosity.

Greek Symbols

e	overall porosity of a mixed bed.
e_D	fractional porosity of the large size particle fraction.
e_d	fractional porosity of the small size particle fraction.
$e_{\min}$	minimum porosity of a mixed bed.
e_{Min}	absolute minimum porosity of a mixed bed.
e_D^0	porosity of a uniform bed of large particles.
e_d^0	porosity of a uniform bed of small particles.
e_{dc}^0	corrected porosity of a uniform bed of small particles.
d	particles size ratio, $d = d / D$.
Δp	pressure drop (Pa).
m	liquid viscosity (Pa·s).

Reference List

1. Ouchiyama, N.; Tanaka, T. Porosity of mass of solid particles having a range of sizes *Ind. Eng. Chem. Fundam.* **1981,** *20*(1), 66-71.
2. Yu, A. B.; Zou, R. P.; Standish, N. Modifying the linear packing model for predicting the porosity of nonspherical particle mixtures *Ind. Eng. Chem. Res.* **1996,***35*(10), 3730-3741.
3. Hulewicz, Z. Z. Resistance to flow through a granular bed in the laminar regime. I. Derivation of a new correlating equation *Int. Chem. Eng.* **1987,** *27*(3), 566-573.
4. Suzuki, M.; Makino, K.; Yamada, M.; Iinoya, K. A study on the coordination number in a system of randomly packed, uniform-sized spherical particles *Int. Chem. Eng.* **1981,** *21*(3), 482-488.
5. Gotoh, K.; Chuba, T.; Suzuki, A. Computer simulation of weight distributions of spherical-particle beds on the bottom of a container *Int. Chem. Eng.* **1982,***22*(1), 107-115.

6. Kuramae, M. Investigation of unsaturated liquid flow in a granular bed using a cubic-lattice pore model *Int. Chem. Eng.* **1982,** *22*(4), 666-673.
7. Yu, A. B.; Standish, N. Estimation of the porosity of particle mixtures by a linear-mixture packing model *Ind. Eng. Chem. Res.* **1991,***30*(6), 1372-1385.
8. Macé, O.; Wei, J. Diffusion in random particle models for hydrodemetalation catalysts *Ind. Eng. Chem. Res.* **1991,** *30*(5), 909-918.
9. MacDonald, M. J.; Chu, C.-F.; Pierre, P. P.; Ng, K. M. A generalized Blake-Kozeny equation for multisized spherical particles *AIChE Journal* **1991,***37*(10), 1583-1588.
10. Mota, M.; Teixeira, J.A.; Yelshin, A. Binary spherical particle mixed beds porosity and permeability relationship measurement *Transactions of the Filtration Society* **2001,** *1*(4), 101-106.
11. Ben Aim, R.; Legoff, P.; Lelec, P. La perméabilité de milieux poreux formés par empilement de mélanges binaires de grains sphériques *Powder Technology* **1971,***5*(1), 51-60.
12. Mota, M.; Teixeira, J.A.; Yelshin, A. Image analysis of packed beds of spherical particles of different sizes *Separation and Purification Technology* **1999,** *15* (15), 59-68.
13. Mota, M.; Teixeira, J.A.; Yelshin, A.; Bowen, W.R. Interfering of coarse particles with finest of different shape in cake model *Minerals Engineering* **2003,** *16*(2), 135-144.
14. Mota, M.; Teixeira, J. A.; Bowen, R.; Yelshin, A. Effect of tortuosity on transport properties of mixedgranular beds, In *Proceedings of 8-th World Filtration Congress, 3-7 April 2000*, Proceedings of 8-th World Filtration Congress, 3-7 April 2000; Filtration Society: Brighton, UK, 2000; Vol. 1, pp. 57-60.
15. Abe, E.; Hirosue, H. Porosity estimation of a mixed cake in body filtration *Journal of Chemical Engineering of Japan* **1982,** *15*(6), 490-493.
16. Dias, R.; Teixeira, J.A.; Mota, M.; Yelshin, A. Effect of the large size ratio in particle binary mixtures on the packing porosity *Ind. Eng. Chem. Res.* **2004,** sent for publishing, pp. 1-30.
17. Currie, J.A. Gaseous diffusion in porous media. Part 2. - Dry granular materials *Brit. J. Appl. Phys.* **1960,** *11*, 318-324.

18. Satterfield, C. N. *Mass Transfer in Heterogeneous Catalysis;* M.I.T. Press: Cambridge, England, 1970.
19. Sharma, R. K.; Cresswell, D. L.; Newson, E. J. Effective diffusion coefficients and tortuosity factors for commercial catalysts *Ind. Eng. Chem. Res.* **1991,** *30*(7), 1428-1433.
20. Aris, R. *The Mathematical Theory of Diffusion and Reaction in Permeable Catalysts;* Clarendon Press: Oxford, 1975; Vol. 1.
21. Satterfield, C. N. *Heterogeneous Catalysis in Practice;* McGraw-Hill: 1980.
22. Geankopolis, C. J. *Transport Processes and Unit Operations;* Allyn and Bacon: USA, 1983.
23. Welty, J. R.; Wicks, C. E.; Wilson, R. E. *Fundamentals of Momentum, Heat, and Mass Transfer;* John Wiley: Singapore, 1984.
24. Rosner, D. E. *Transport Processes in Chemically Reacting Flow Systems;* Butterworths: USA, 1986.
25. Olague, N. E.; Smith, D. M.; Ciftcioglu, M. Knudsen diffusion in ordered sphere packings *AIChE Journal* **1988,** *34*(11), 1907-1909.
26. Walas, S. M. *Chemical Reaction Engineering Handbook of Solved Problems;* Gordon & Breach Pub.: Amsterdam, 1995.
27. Blanch, H. W.; Clark, D. S. *Biochemical Engineering;* M.Dekker: New York, 1996.
28. Revil, A. Ionic diffusivity, electrical conductivity, membrane and thermoelectric potentials in colloids and granular porous media: a unified model *J. Colloid and Interface Sci.* **1999,** *212*(2), 503-522.
29. Klusácek, K.; Schneider, P. Effect of size and shape of catalyst microparticles on pellet pore structure and effectiveness *Chem. Eng. Sci.* **1981,** *36*(3), 523-527.
30. Huizenga, D. G.; Smith, D. M. Knudsen diffusion in random assemblages of uniform spheres *AIChE Journal* **1986,** *32*(1), 1-6.
31. Wright, T.; Smith, D. M.; Stermer, D. L. Knudsen diffusion in bidisperse mixtures of uniform spheres *Ind. Eng. Chem. Res.* **1987,** *26*(6), 1227-1232.
32. Mota, M.; Teixeira, J. A.; Yelshin, A. Tortuosity in bioseparations and its application to food processes, In *Proceedings of 2nd European Symposium on Biochemical*

Engineering Science, Porto, 16-19 Sept. 1998, Feyo de Azevedo; Ferreira, E.; Luben, K.; Osseweijer, P., Eds.; Univ. of Porto: Porto, Portugal, 1998; pp. 93-98.

33. Mota, M.; Teixeira, J. A.; Keating, J. B.; Yelshin, A. Modelling changes in diffusion through the brain extracellular space, In *European Symposium on Biochemical Engineering Science (ESBES-4), Delft, The Netherlands, 29-31 August 2002*, *European Symposium on Biochemical Engineering Science (ESBES-4)*, Delft, The Netherlands, 29-31 August 2002; Delft, 2002; pp. 11.
34. Mota, M.; Teixeira, J.A.; Yelshin, A. Immobilized particles in gel matrix-type porous media. Homogeneous porous media model *Biotechnology Progress* **2001,** *17*(5), 860-865.
35. Mathias, M.F.; Muldowney, G.P. Effect of solids loading method on the bed porosity and gas flux distribution in a fixed-bed reactor *Chem. Eng. Sci.* **2000,** *55*(21), 4981-4991.
36. Zhang, Z.P.; Yu, A.B.; Oakeshott, R.B.S. Effect of packing method on the randomness of disc packings *J. Phys. A: Math. Gen.* **1996,** *29*, 2671-2685.
37. Wightman, C.; Mort, P. R.; Muzzio, F. J.; Riman, R. E.; Gleason, E. K. The structure of mixtures of particles generated by time-dependent flows *Powder Technology* **1995,** *84*(3), 231-240.
38. Al-Dahhan, M.H.; Wu, Y.; Dudukovic, M.P. Reproducible technique for packing laboratory-scale trickle-bed reactors with a mixture of catalyst and fines *Ind. Eng. Chem. Res.* **1995,** *34*(3), 741-747.
39. Zou, R.P.; Yu, A.B. Evaluation of the packing characteristics of mono-sized non-spherical particles *Powder Technology* **1996,** *88*, 71-79.
40. Dias, R.; Teixeira, J.A.; Mota, M.; Yelshin, A. Preparation of controlled particulate mixtures with glass beads of different sizes *Separation and Purification Technology* **2003,** *Article MS 20-46, in press.*
41. Liu, S.; Ha, Z. Prediction of random packing limit for multimodal particle mixtures *Powder Technology* **2002,** *126*, 283-296.
42. Yu, A.B.; Zou, R.P.; Standish, N. Packing of ternary mixtures of non-spherical particles *J. Am. Ceram. Soc.* **1992,** *75*, 2765-2772.

43. Ouchiyama, N.; Tanaka, T. Porosity estimation for random packings of spherical particles *Ind. Eng. Chem. Fundam.* **1984,** *23*(4), 490-493.
44. Yu, A. B.; Standish, N. A study of the packing of particles with a mixture size distribution *Powder Technology* **1993,** *76*, 113-124.
45. Milewski, J. V. The combined packing of rods and spheres in reinforcing plastics *Ind. Eng. Chem. Prod. Res. Dev.* **1978,** *17*(4), 363-366.
46. Mota, M.; Teixeira, J.A.; Yelshin, A. Image modelling of mixed granular porous media *Fluid/Particle Separation Journal* **1999,** *12* (2), 71-79.
47. Yelshin, A.; Mota, M.; Teixeira, J. Porous media behaviours modelling and analysis in separation processes, In *Proceedings of Int. Conference Filtech Europa-97, Düsseldorf, Germany, October 14 – 16 1997*, *Proceedings of Int. Conference Filtech Europa-97*, Düsseldorf, Germany, October 14 – 16 1997; Filtration Society: Horsham (UK), 1997; pp. 327-334.
48. Bentz, D.P.; Garboczi, E.J. Simulation studies of the effects of mineral admixtures on the cement past-aggregate interfacial zone *Amer. Concrete Institute Materials Journal* **1991,** *88,* 518-529.
49. Garboczi, E.J.; Bentz, D.P. Digital simulation of the aggregate-cement past interfacial zone in concrete *Journal of Material Research* **1991,** *6*, 196.